Science and Technology for Energy Transition **79**, 75 (2024)

https://doi.org/10.2516/stet/2024081

Available online at:
stet-review.org

Emerging Advances in Hybrid Renewable Energy Systems and Integration
Muhammad Zakarya, Santosh Tirunagari, Jinguang Han and Peiying Zhang (Guest Editors)

REGULAR ARTICLE OPEN ACCESS

Synergistic adaptive control of virtual inertia and damping coefficient in virtual synchronous generators for standalone microgrid applications

Nengwang Xie[1], Jinning Liu[1,*], Yong Wang[1], ZhiYong Yin[1], Caixue Chen[2], and Lihao Wang[1]

[1] Shijiazhuang Campus of Army Engineering University of PLA, Shijiazhuang 050000, PR China
[2] Xiangtan University, Xiangtan 411100, PR China

Received: 8 July 2024 / Accepted: 3 September 2024

Abstract. The current control methods for virtual synchronous generators (VSG) in regulating inverter frequency in standalone microgrids at border posts and remote mountainous regions remain suboptimal. This study introduces a small-signal VSG model to elucidate the intrinsic dynamics of the virtual inertia and damping coefficient, along with their coupled interrelationship. A novel VSG control approach is proposed, featuring synergistic adaptive regulation of both virtual inertia and damping coefficient. This approach is designed to optimize the interaction of the virtual inertia and damping coefficient with the frequency difference and rate of frequency variation, within a predefined operational range. Additionally, it adaptively modulates these parameters to mitigate further frequency reductions, taking into account the frequency difference and active power when deviations occur outside the predefined range. The experiments demonstrate that this approach effectively moderates the rate of frequency change, diminishes frequency departure velocity for approximately 4 times the original during disturbances, expedites frequency stabilization post-disturbance, the stabilization time is reduced by at least half of the original and prevents excessive frequency deviations. The implementation of this method significantly enhances the response speed and accuracy of frequency control in standalone microgrids, contributing to improved overall system stability.

Keywords: Damping coefficient, Standalone microgrid, Synergetic adaptive control, Virtual inertia.

1 Introduction

The advent of novel energy technologies and escalating electricity demands have spurred the use of standalone microgrids in regions devoid of main grid connectivity, including high plateaus, sea islands, and isolated rural locales. The concept of the virtual synchronous generator (VSG), pioneered by Italian researchers [1], has gained widespread adoption for frequency regulation in these microgrids. Distinct from traditional control methodologies, the VSG offers enhanced inertia support and superior transient response capabilities [2], effectively addressing the challenges of absent or low inertia in independent microgrids [3]. Typically, the VSG's regulation of virtual inertia and damping coefficient is based on a synthesis of automatic control theory with empirical knowledge [4]. However, the prevalent fixed-parameter approach of VSG operation has shown limitations in adaptability to varying loads, resulting in constrained frequency regulation capacity and reduced control flexibility.

In contrast to the fixed parameters of conventional synchronous generators [5], the VSG's inertia and damping coefficients can be dynamically adjusted to suit specific operational contexts [6]. Recent advancements include an automated virtual inertia regulation method based on real-time power input signals and system frequency deviations [7], significantly enhancing frequency response speed and providing increased inertia for improved frequency stability during power and frequency disturbances [8]. An advanced VSG model incorporating an enhanced torque governor with angular frequency inertia has been developed [9], effectively diminishing the rate of frequency variation. Additionally, an adaptive approach that concurrently considers the damping coefficient and virtual inertia have been proposed [10], augmenting dynamic frequency response and mitigating the extent of frequency reductions. A novel adaptive inertia strategy, which utilizes the benefits of both high and low inertia, has been introduced [11], facilitating a rapid frequency recovery and enhancing the microgrid's resilience to disturbances. However, challenges remain, as evidenced by the impact of virtual impedance on bus voltage stability [12], and the intricacies of balancing

* Corresponding author: harmony2013@163.com

rotational inertia with virtual impedance for frequency stability. In response, a hybrid control method combining adaptive inertia and damping, integrated with interleaving control techniques, has been proposed to further refine frequency stability.

To improve the stability and adaptability of VSG control, substantial research has been dedicated to utilizing virtual inertia to decelerate frequency variation rates and expedite the return to steady-state conditions [13]. However, these methods often overlook the adjustable spectrum of system inertia and the consequential effects arising from the interplay between virtual inertia and damping coefficient. Furthermore, the majority of adaptive control strategies for VSG parameters, which feature adaptive regulation, are predominantly tailored for grid-connected microgrids, with scant attention to standalone microgrids. In light of these challenges, we introduce a novel adaptive VSG control approach, characterized by the synergistic and adaptive regulation of both virtual inertia and damping coefficient (termed synergetic adaptive VSG control).

2 Analysis of the VSG control mechanism

The VSG plays a pivotal role in stabilizing the frequency of microgrids by emulating the external characteristics of conventional synchronous generators [14]. In comparison to droop control [15] and voltage-frequency (VF) control [16], VSG control is distinguished by its incorporation of virtual inertia response and damping effect, attributes that significantly contribute to the enhanced transient stability of microgrids [17].

The VSG's unique advantages stem from its integration of virtual inertia and damping coefficient, providing both inertia support and damping effects during transient phases [18]. the active power can be decomposed into components generated by virtual inertia, ΔPJ, and those by the damping coefficient, ΔP_D. Consequently, the equations can be derived:

$$\Delta P_G = 2\pi D w_n \Delta f + 2\pi J w_n \frac{df}{dt}, \tag{1}$$

$$\Delta P_J = 2\pi J w_n \frac{df}{dt}, \tag{2}$$

$$\Delta P_D = 2\pi D w_n \Delta f, \tag{3}$$

where $\Delta P_G = P_{ref} - P$ signifies the inverter's output active power, w_n is the rated angular velocity, $\Delta f = (w - w_0)/2\pi$ is the frequency difference, and f is the inverter's transient frequency.

During transient load disturbances, ΔP_G remains constant and Δf is typically minimal. Consequently, equation (4) can be inferred from (1). In this transient state, the role of virtual inertia becomes paramount in controlling the rate of frequency variation. An increase in virtual inertia correlates with a reduced rate of frequency variation.

$$\Delta P_G = \Delta P_J \approx 2\pi J w_n \frac{df}{dt}. \tag{4}$$

As the rate of frequency change accelerates, the frequency difference (Δf) increases, which leads to a corresponding decrease in the frequency variation rate. When Δf reaches a substantial value or stabilizes at a new steady state, the frequency variation rate nears zero, as outlined in equation (5). In this state, the damping coefficient assumes a dominant role in determining the magnitude of Δf. Consequently, an increased damping coefficient results in a reduced Δf. Utilizing this characteristic, Δf can be effectively controlled within a predetermined range through the adaptive adjustment of the inverter's damping coefficient.

$$\Delta P_G = \Delta P_D \approx 2\pi D w_n \Delta f. \tag{5}$$

The interplay between virtual inertia and damping coefficient is crucial in shaping the system's frequency response during power disturbances, with each alternately assuming prominence. This dynamic indicates an inherent coupling relationship between the two, akin to the function of a proportional-derivative (PD) controller, where J and D correlate to the proportional and derivative gains, respectively.

To enhance the understanding of the VSG operation and its impact on the stability of the microgrid [19], the small-signal analysis illustrates that as J increases, the pole gravitates towards the imaginary axis, paradoxically leading to heightened system instability. This outcome is contrary to the initial objective of augmenting virtual inertia to enhance the system's inertia support. Conversely, an increase in D enhances the damping effect, propelling the pole further from the imaginary axis, and thereby bolstering system stability. However, a higher D also leads to an increased steady-state error, necessitating adaptive control of D to maintain acceptable power quality. The insights from this characteristic analysis underpin the development of a VSG control methodology that adaptively regulates virtual inertia and damping coefficient, based on their operational mechanisms and their interrelated dynamics [20].

Building upon this small-signal analysis, it is imperative to ascertain the relationship between J and D and their optimal value ranges in accordance with the system's actual parameter regulation capabilities. This involves utilizing the second-order transfer function $G(s)$ of the active power circuit, derived from the small-signal analysis, to investigate system dynamic-performance metrics, specifically the angular frequency of natural vibration (w_z) and the damping ratio (ε). The analysis revealed that while virtual inertia predominantly influences w_z, both virtual inertia and damping coefficient concurrently affect ε. The relationships between these parameters are encapsulated in the following equations:

$$w_z = \sqrt{\frac{E_0 U}{J w_n Z}}, \tag{6}$$

$$D = \frac{2\varepsilon}{\sqrt{\frac{\omega_0 Z}{J E_0 U_l}}}. \tag{7}$$

The configuration of J typically draws inspiration from conventional synchronous generators, with the angular frequency of natural vibration (w_z) set within the range of

0.628–15.700. This allows for the determination of the optimal value range for J, denoted as $[J_{min}, J_{max}]$. In alignment with principles of automatic control theory, the damping ratio (ε) is set to 0.707, recognized as the optimal damping ratio for a second-order system. Consequently, the desired value range for the damping coefficient (D), $[D_{min}, D_{max}]$, is computed using equation (7).

These defined value ranges for virtual inertia and damping coefficient serve as constraints in the synergetic adaptive VSG control method, providing theoretical benchmarks for setting VSG control parameters. Additionally, under circumstances where system frequency deviation reaches its upper threshold, an alternate mode is employed to regulate the damping coefficient. In this mode, the damping coefficient operates independently of the virtual inertia and is permitted to surpass its predefined limits, thereby optimizing frequency stability.

3 Synergetic adaptive VSG control method

The small-signal analysis of the VSG underscores the significant impact of virtual inertia on the transient frequency response. Accordingly, the adaptive control of parameters is based on the following core principle: an increase in virtual inertia is employed to curb frequency variations and slow down their rate when the frequency deviates from the rated value. Conversely, during the frequency recovery phase, virtual inertia is reduced to accelerate the frequency variation rate and hasten the frequency normalization process. This principle guides the adaptive regulation of virtual inertia, which is articulated as follows:

$$J_{min} < J = k_J * s * f * (f - f_n) + J_{min} < J_{max}, \tag{8}$$

where J represents the virtual inertia of the inverter, k_J is the gain coefficient, f is the transient frequency, f_n is the rated frequency, and s is the complex frequency domain differential operator. It is also crucial to set the virtual inertia to its maximum during significant load fluctuations. The gain coefficient k_J is thus determined using the subsequent equation:

$$k_J = \frac{2\pi * w_n * J_{max}(J_{max} - J_{min})}{\Delta P_J \Delta f_{max}}, \tag{9}$$

where Δf_{max} represents the maximum frequency deviation.

The damping coefficient in VSG control functions analogously to the primary first-order frequency regulation observed in conventional synchronous generators [21]. It is instrumental in determining the extent of frequency adjustment required for reestablishing the steady state following load variations. For standalone microgrids, it is crucial that the maximum frequency fluctuation Δf_{max} remains below a predetermined threshold. In this study, f_{max} is set at 0.3 Hz, in accordance with the GJB 235B-2020 specifications applicable to Class III electrical stations.

Consequently, during typical operations of a standalone microgrid, Δf is expected to be less than Δf_{max}. If Δf surpasses this pre-established range, the adaptive regulation of the damping coefficient (D) can be determined by incorporating the maximum load variation ΔPG and the maximum frequency deviation Δf_{max} into equation (5). When Δf remains within the predefined range, the interplay between the damping coefficient and virtual inertia must adhere to equation (7), reflecting their coupling relationship. The following constraints are thus applicable to the damping coefficient in the complex frequency domain:

$$D = \begin{cases} k_D * (f_i - f) * \dfrac{K_i}{s} + 2\varepsilon\sqrt{\dfrac{JE_0U}{\omega_0 Z}} & \Delta f < \Delta f_{max} \\ \dfrac{\Delta P_G}{2\pi w_n \Delta f_{max}} & \Delta f \geq \Delta f_{max} \end{cases}, \tag{10}$$

where $f_i = f_{min}$ when $f < 50$ Hz, and $f_i = f_{max}$ otherwise. K_D is set to 0 when $\Delta f < \Delta f_{max}$, and to 1 otherwise. K_i represents the damping integral coefficient.

To maintain frequency fluctuations within the specified limits during substantial load changes, the following equation is derived, based on the final value theorem:

$$K_i = \frac{D_{max} - 2\varepsilon\sqrt{\frac{JE_0U}{\omega_0 Z}}}{f_i - f}. \tag{11}$$

When the frequency deviation remains below the predetermined maximum fluctuation, the proposed method adeptly regulates virtual inertia and damping coefficients within their respective optimal ranges. This synergetic adaptive control is meticulously attuned to frequency fluctuations, effectively decelerating frequency deviation during system disturbances and facilitating rapid frequency stabilization post-disturbance. In scenarios where the frequency deviation surpasses the specified maximum, a specialized control mode for the damping coefficient is activated, designed to curtail further frequency divergence.

4 Experimental validation

The novel VSG control strategy introduced here distinctively manages both the rate and magnitude of frequency variation by utilizing the flexible adjustability of virtual inertia and damping coefficient. Employing equations (6) and (7), the calculated desirable ranges for virtual inertia and damping coefficient were determined to be 0.0062–3.869 and 0.135–84.15, respectively. The resistor is 0.05 **Ω**, filter inductor is 2 mH, filter capacitor is 0.01 mF.

4.1 Experimental validation with resistive load

To assess the efficacy of the proposed VSG control method under resistive load conditions, the maximum frequency deviation Δf_{max} was set to 0.8 Hz. In this simulation scenario, the inverter power command was established at 40 kW, with the system initially bearing a 40 kW resistive load. A comparative analysis was then conducted by introducing an additional 50 kW power load. For this comparative study, the VSG control with constant parameters was employed. Set the fixed virtual inertia J1 to 0.62 kg·m^2 and the fixed damping coefficient D1 to 16.88 N·s/m.

Figure 1(a) shows a notable short-term overshoot of 11.2 kW in P1 at the moment of increasing the load by

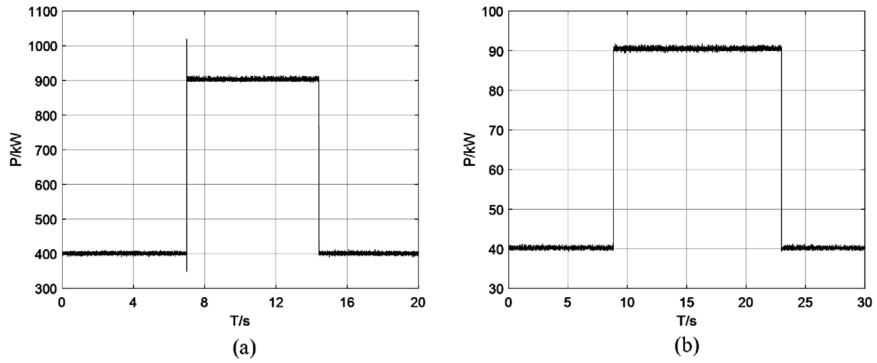

Figure 1. Comparative power fluctuation graphs with 50 kW load variation under different VSG controls. (a) Constant-parameter VSG control. (b) Adaptive VSG control.

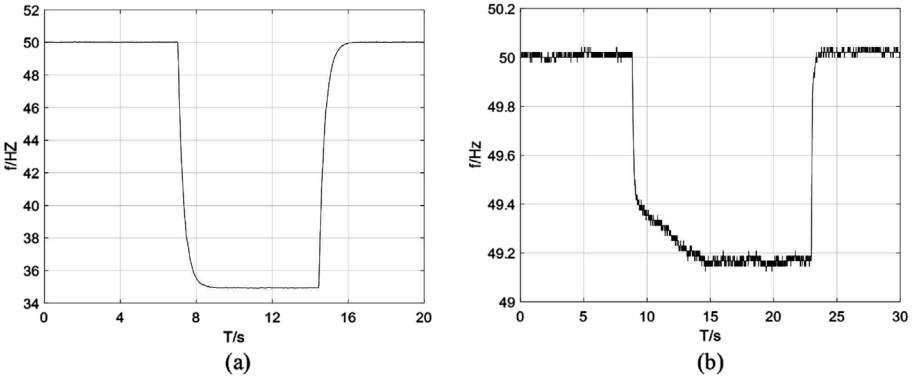

Figure 2. Comparative frequency fluctuation graphs with 50 kW load variation under different VSG controls. (a) Constant-parameter VSG control. (b) Adaptive VSG control.

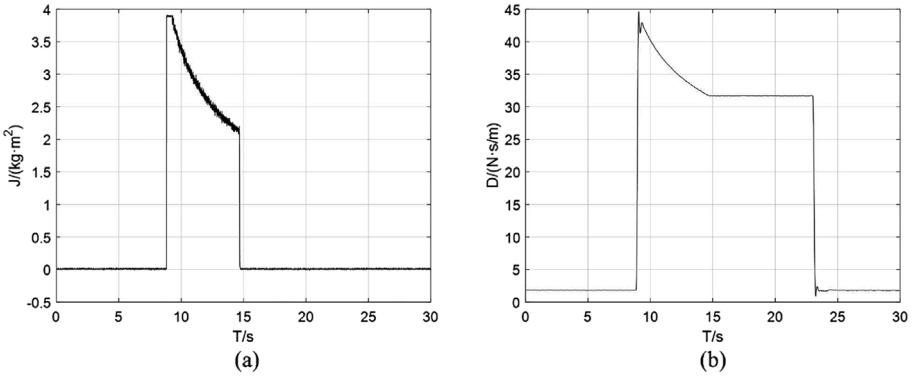

Figure 3. *Fluctuation* graphs of virtual inertia and damping coefficient during 50 kW power variation. (a) Virtual inertia (J) fluctuation. (b) Damping coefficient (D) fluctuation.

50 kW. In contrast, Figure 1(b) shows that P2 experienced no overshoot, which corroborates the effectiveness of adaptive control in preventing instantaneous power overloads.

Figures 2 and 3 depict the frequency response during the process of load increase and decrease. For f_1, the frequency took 1.8 s to decrease from 50 Hz to 35.4 Hz and subsequently 1.6 s to return to 50 Hz. Concurrently, f_2 exhibited an increase in virtual inertia to 3.869 kg·m^2 following the load increase, before reverting to its initial value. The damping coefficient (D) rose to 44.6 N·s/m and then stabilized at 31.6 N·s/m, effectively decelerating the rate of decrease in f_2. It took 5.7 s for the frequency to drop from 50 Hz to 49.2 Hz, after which it maintained stability. Upon load reduction, the damping coefficient reverted to its initial value, leading to an accelerated recovery of f_2 in 0.75 s.

Table 1. Parameter setting for simulating the system subjected to electric motor loads.

Parameter	Value	Parameter	Value	Parameter	Value
P_{Dref}/kW	3.0000	$J_M/kg \cdot m^2$	0.0001	P_1/kW	3.0000
$J_1/kg \cdot m^2$	0.0062	$D_1/(N \cdot s/m)$	1.3500	P_2/kW	3.0000

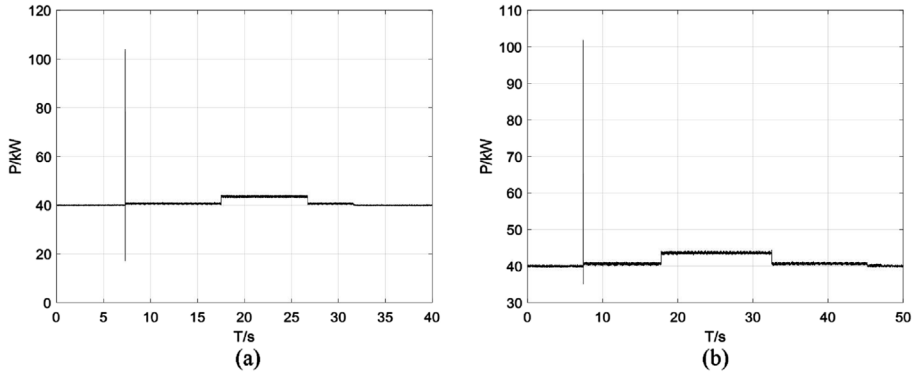

Figure 4. Comparative power waveform graphs with motor load under different VSG controls. (a) Constant-parameter VSG control. (b) Adaptive VSG control.

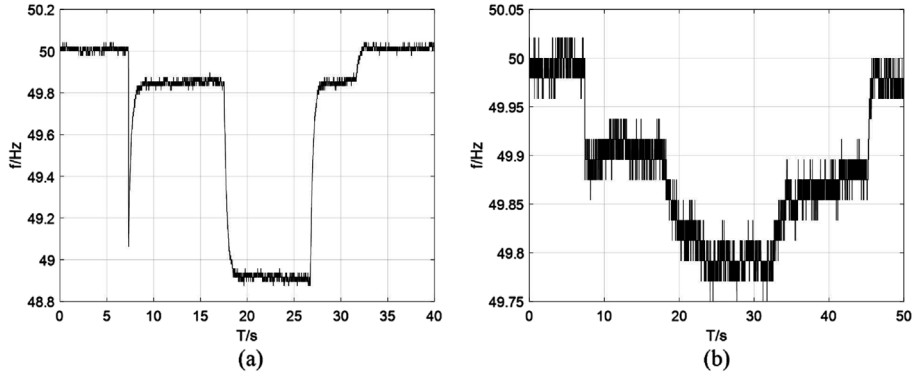

Figure 5. Frequency waveform graphs of inverter with motor load under different VSG control methods. (a) Constant-parameter VSG control. (b) Adaptive VSG control.

4.2 Experimental validation with motor load

To evaluate the proposed method's performance under motor load conditions, Δf_{max} was set to 0.2 Hz. The inverter power command was fixed at 40 kW with an initial 40 kW load. A comparative analysis was performed involving the simultaneous application of a 1 kW resistive load and the initiation of a 3 kW motor under no load, followed by a 3 kW increase in motor power. Specific parameters are detailed in Table 1.

P_{Dref} is the rated power of the electric motor load, P_1 to the load on the electric motor at startup, and P_2 to the additional load applied. J_M denotes the rotational inertia of the electric motor.

Observations from Figure 4 through Figure 6 indicate that at the instance of the motor's no-load start, P1 experienced a change of 87 kW, causing f_1 to initially drop to 49.05 Hz before recovering to 49.75 Hz. P2 underwent a change of 66.7 kW, with f_2 decreasing to 49.9 Hz. This result demonstrates the proposed method's capability in effectively mitigating issues related to motor start-up overload and rapid frequency drops, highlighting its robustness and adaptability under varying load conditions, including those involving motor startups.

Upon introducing an additional 3 kW load to the motor, the frequency response f_1 decreased over a span of 2.4 s from 49.75 Hz to 48.9 Hz and subsequently took 2 s to recover back to 50 Hz. In the case of f_2, following the load increase, the virtual inertia (J) escalated to 0.85 kg·m^2 before returning to its baseline value. Concurrently, the damping coefficient (D) increased to 19.3 N·s/m and then stabilized at 9 N·s/m, effectively slowing down the rate at which f_2 decreased. The frequency required 6 s to diminish from 49.9 Hz to 49.8 Hz and subsequently maintained stability. When the load was decreased, D reverted to its initial value, enabling f_2 to accelerate its recovery within 2 s. These experimental outcomes are detailed in Table 2.

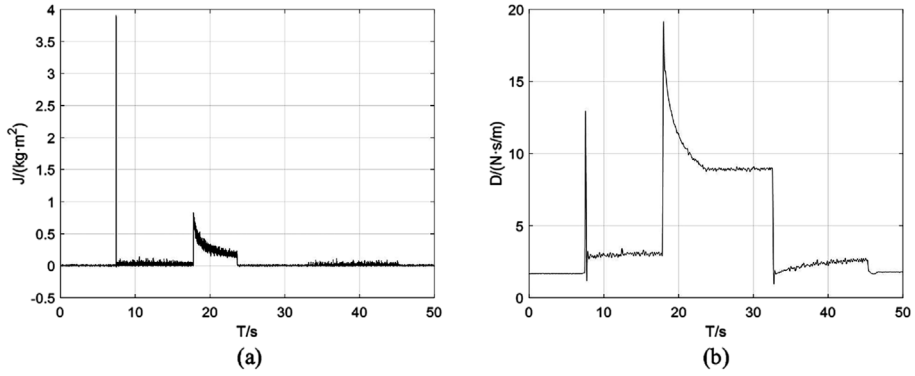

Figure 6. Fluctuation graphs of virtual inertia and damping coefficient during inverter operation with motor load. (a) Virtual inertia fluctuation. (b) Damping coefficient fluctuation.

Table 2. Experimental conclusions with motor load for two control methods.

Parameters	J&D constant	J&D adaptive
Instantaneous power change at startup (kW)	87.00	66.70
Instantaneous frequency change at startup (Hz)	0.95	0.10
Frequency decrease duration after load increase (s)	2.40	6.00
Frequency change after load increase (Hz)	0.85	0.10
Frequency recovery duration after load decrease (s)	2.00	2.00
Frequency change after load decrease (Hz)	1.10	0.20

Table 3. Parameter setting for simulations of a system subjected to a pulse load.

Parameter	Value	Parameter	Value	Parameter	Value
P_{MCref}/kW	20.000	T/s	0.0100	T_0/s	0.0030

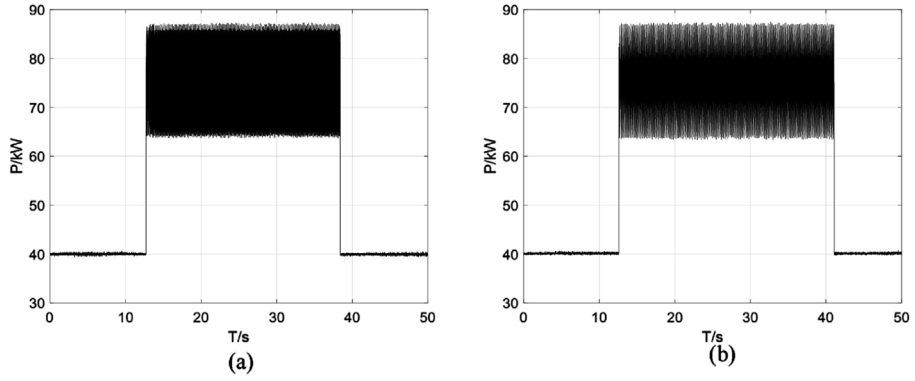

Figure 7. Power waveform graphs of inverter with pulsating load under different control methods. (a) Constant-parameter VSG control. (b) Adaptive VSG control.

4.3 Experimental validation with pulsating load

To evaluate the method's performance under pulsating load conditions, Δf_{max} was set to 0.4 Hz. The inverter's power command was established at 40 kW, with an initial 40 kW load. A comparative analysis was undertaken by applying a pulsating load with a peak power of 20 kW and employing constant-parameter VSG control. The specific parameters for this setup are provided in Tables 1 and 3. T is the pulse period, and T_0 is the pulse width.

Figure 7 demonstrates that both control method did not significantly impact power. Figures 8 and 9 illustrate that after introducing the pulsating load, f_1 required 2.5 s to

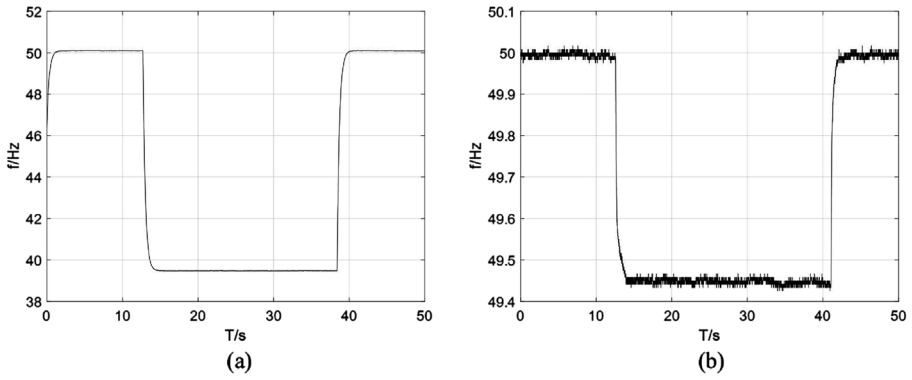

Figure 8. Frequency waveform graphs of inverter with pulsating load under different control methods. (a) Constant-parameter VSG control. (b) Adaptive VSG control.

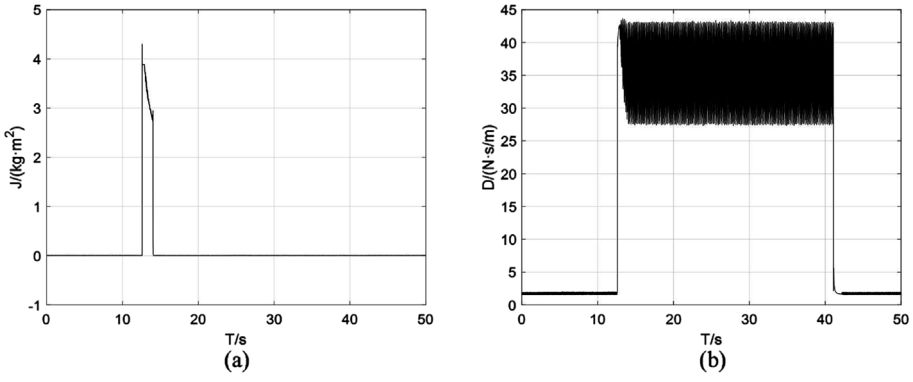

Figure 9. Fluctuation graphs during inverter operation with the pulsating load. (a) Virtual inertia fluctuation. (b) Damping coefficient fluctuation.

decrease from 50 Hz to 39.44 Hz and an equal duration to return to 50 Hz.

After the load increase, J rose to 3.88 kg·m^2 before diminishing to its original value. Simultaneously, D increased to 40.85 N·s/m and eventually reached its threshold. As the power pulsated, f_2 stabilized at 49.6 Hz. During this period, the rate of decrease in f_2 was moderated. It took 1 s for the frequency to drop from 50 Hz to 49.6 Hz, after which it sustained stability. With the load reduction, D reverted to its initial value, facilitating a quicker recovery for f_2 within 2 s.

5 Conclusion

The traditional VSG control methodologies have shown limitations in fully utilizing the flexible adjustment of virtual inertia and damping coefficient for enhancing frequency control capabilities in standalone microgrid systems. It is easy to cause stability problems caused by improper setting of virtual inertia and damping coefficient. To address this limitation, we developed a novel VSG control approach that features synergetic adaptive regulation of virtual inertia and damping. This method meticulously considered the intrinsic coupling relationship between frequency difference, frequency variation rate, virtual inertia, and damping coefficient, in addition to the magnitude of power variations. By strategically optimizing the settings of virtual inertia and damping coefficient, our proposed technique effectively managed both temporal and spatial frequency variations within predefined ranges under diverse load conditions, thereby substantially improving the operational stability of standalone microgrids. The significance of this method was particularly pronounced in remote or border areas, where varied loads such as radars and motors were prevalent. The versatility of our approach lies in its ability to effectively mitigate frequency deviations, expedite frequency recovery, and constrain frequency differences. Consequently, this method presents a robust solution to the challenges of frequency stability in standalone microgrid systems, ensuring consistent and reliable power delivery across a spectrum of operational scenarios. This advancement marks a significant stride in microgrid technology, offering a more dynamic and responsive control mechanism that caters to the evolving demands of modern electrical systems. However, this method only adjusts the two parameter values from the perspective of the source side response. If the variable inertia requirements of the system can be combined, the VSG performance can be further developed and the reliability can be improved.

Conflicts of interest

The authors declare no conflicts of interest.

Data availability statement

The participants of this study did not give written consent for their data to be shared publicly, so due to the sensitive nature of the research supporting data is not available.

References

1 Driesen J., Visscher K. (2008, July 1) Virtual synchronous generators, in: *IEEE power and energy society general meeting – conversion and delivery of electrical energy*, Pittsburgh, PA, USA, pp. 1–3. https://doi.org/10.1109/PES.2008.4596800.

2 Liu J., Miura Y., Bevrani H., Ise T. (2017) Enhanced virtual synchronous generator control for parallel inverters in microgrids, *IEEE Trans. Smart Grid* **8**, 2268–2277. https://doi.org/10.1109/TSG.2016.2521405.

3 Hirase Y., Sugimoto K., Sakimoto K., Ise T. (2016) Analysis of resonance in microgrids and effects of system frequency stabilization using a virtual synchronous generator, *IEEE J. Emerg. Sel. Top. Power Electron.* **4**, 1287–1298. https://doi.org/10.1109/JESTPE.2016.2581818.

4 Hirase Y., Abe K., Sugimoto K., Sakimoto K., Bevrani H., Ise T. (2018) A novel control approach for virtual synchronous generators to suppress frequency and voltage fluctuations in microgrids, *Appl. Energy* **210**, 699–710. https://doi.org/10.1016/j.apenergy.2017.06.058.

5 Yang X., Song Y., Wang G., Wang W. (2010) A comprehensive review on the development of sustainable energy strategy and implementation in China, *IEEE Trans. Sustain. Energy* **1**, 57–65. https://doi.org/10.1109/TSTE.2010.2051464.

6 Chen Y., Hesse R., Turschner D., Beck H. (2011) Improving the grid power quality using virtual synchronous machines, in: *International conference on power engineering, energy and electrical drives*, Málaga, Spain, pp. 1–6. https://doi.org/10.1109/PowerEng.2011.6036498.

7 Kerdphol T., Watanabe M., Hongesombut K., Mitani Y. (2019) Self-adaptive virtual inertia control-based fuzzy logic to improve frequency stability of microgrid with high renewable penetration, *IEEE Access* **7**, 76071–76083. https://doi.org/10.1109/ACCESS.2019.2920886.

8 Shi K., Chen C., Sun Y., Xu P., Yang Y., Blaabjerg F. (2020) Rotor inertia adaptive control and inertia matching strategy based on parallel virtual synchronous generators system, *IET Gener. Transm. Distrib.* **14**, 1854–1861. https://doi.org/10.1049/iet-gtd.2019.1394.

9 Zhu F., Peng Z., Hu W., Wang H., Zhang C., Zhao Z., Dai Y. (2021) An improved VSG control strategy for microgrid, in: *IEEE international conference on electrical engineering and mechatronics technology (ICEEMT)*, Qingdao, China, pp. 338–342. https://doi.org/10.1109/ICEEMT52412.2021.9602085.

10 Rathore B., Chakrabarti S., Anand S. (2016) Frequency response improvement in microgrid using optimized VSG control, in: *National power systems conference (NPSC)*, Bhubaneswar, India, pp. 1–6. https://doi.org/10.1109/NPSC.2016.7858916.

11 Hou X., Han H., Zhong C., Yuan W., Yi M., Chen Y. (2016) Improvement of transient stability in inverter-based AC microgrid via adaptive virtual inertia, in: *IEEE energy conversion congress and exposition (ECCE)*, Milwaukee, WI, USA, pp. 1–6. https://doi.org/10.1109/ECCE.2016.7855195.

12 Li D., Zhu Q., Lin S., Bian X.Y. (2017) A self-adaptive inertia and damping combination control of VSG to support frequency stability, *IEEE Trans. Energy Convers.* **32**, 397–398. https://doi.org/10.1109/TEC.2016.2623982.

13 Li J., Wen B., Wang H. (2019) Adaptive virtual inertia control strategy of VSG for micro-grid based on improved bang-bang control strategy, *IEEE Access* **7**, 39509–39514. https://doi.org/10.1109/ACCESS.2019.2904943.

14 Monica P., Kowsalya M. (2016) Control strategies of parallel operated inverters in renewable energy application: a review, *Renew. Sustain. Energy Rev.* **65**, 885–901. https://doi.org/10.1016/j.rser.2016.06.075.

15 Hajilu N., Gharehpetian G.B., Hosseinian S.H., Poursistani M.R., Kohansal M. (2015) Power control strategy in islanded microgrids based on VF and PQ theory using droop control of inverters, in: *International congress on electric industry automation (ICEIA)*, Shiraz, Iran, pp. 37–42. https://doi.org/10.1109/ICEIA.2015.7165844.

16 Sakimoto K., Miura Y., Ise T. (2011) Stabilization of a power system with a distributed generator by a virtual synchronous generator function, in: *8th international conference on power electronics – ECCE Asia*, Jeju, South Korea, pp. 1498–1505. https://doi.org/10.1109/ICPE.2011.5944492.

17 Chen M., Zhou D., Blaabjerg F. (2020) Modelling, implementation, and assessment of virtual synchronous generator in power systems, *J. Mod. Power Syst. Clean Energy* **8**, 399–411. https://doi.org/10.35833/MPCE.2019.000592.

18 Chen J., O'Donnell T. (2019) Parameter constraints for virtual synchronous generator considering stability, *IEEE Trans. Power Syst.* **34**, 2479–2481. https://doi.org/10.1109/TPWRS.2019.2896853.

19 Feng J., Bai F., Nadarajah M., Ma H. (2023) Transition towards inverter-based generation with VSG control: low frequency instability prospective, in: *2023 IEEE international conference on energy technologies for future grids (ETFG)*, Wollongong, Australia, pp. 1–6. https://doi.org/10.1109/ETFG55873.2023.10407495.

20 Khajesalehi J., Afjei S.E. (2023) Fault-tolerant virtual synchronous generator control of inverters in synchronous generator-based microgrids, *Electr. Power Syst. Res.* **218**, 109173. https://doi.org/10.1016/j.epsr.2023.109173.

21 Kryonidis G.C., Juan M.M., Malamaki K.-N.D., Barragán-Villarejo M., de Paula García-López F., Francisco J.M.-D., José M.M.-O., Demoulias C.S. (2023) Use of ultracapacitor for provision of inertial response in virtual synchronous generator: design and experimental validation, *Electr. Power Syst. Res.* **223**, 109607. https://doi.org/10.1016/j.epsr.2023.109607.